Control of Karman Vortex Street By Using Plasma Actuators

D. O. Redchyts[1], E. A. Shkvar[2, *] and S. V. Moiseienko[3]

Abstract: A mathematical model for unsteady electro- and aerodynamic processes in the presence of a plasma actuator has been elaborated through physical modeling of the dielectric barrier discharge. A specialized computational fluid dynamics package has been developed accordingly in order to calculate steady and unsteady laminar and turbulent flows. For the numerical simulation of the dielectric barrier discharge, in particular, two equations have been added to the Navier-Stokes equations and solved. They describe the distribution of the applied voltage and the charged particles density. The impact of the plasma actuator on air has been accounted for through the Lorentz force, included as a source term in the momentum balance equation. The system of governing equations for the considered hydrodynamics and electrodynamics has been written in an arbitrary curvilinear coordinate system in dimensionless form and integrated in the framework of a finite volume method. A TVD scheme with a third-order ISNAS flow limiter has been chosen for the convective terms approximation. The obtained block-matrix system of linear algebraic equations has been solved by the generalized minimal residual (GMRES) method with ILU(k) preconditioning. Using this approach, the occurrence of a propulsion force, emerging as a result of the action of plasma actuators on a cylinder in quiescent air, has been investigated. The possibility to mitigate the cylinder drag coefficient with the help of the plasma actuators, due to the ensuing suppression of the Karman vortex street, has been demonstrated.

1 Introduction

The air flow control is of considerable interest in connection with the prospects for the development of land transport, aviation, wind power, the creation of new types of gas turbines and other mechanisms. There are many different passive and active techniques of flow control for both drag reduction and stall prevention [Gad-El-Hak (2007); Shkvar, Kryzhanovskyi and Cai (2018)]. One of the promising methods of influencing the laminar or turbulent air flow without the use of consumables is the use of plasma

---

[1] Institute of Transport Systems and Technologies of National Academy of Science of Ukraine, Dnipro, 49005, Ukraine.

[2] College of Engineering, Zhejiang Normal University, Jinhua, 321004, China.

[3] Kherson National Technical University, Kherson, 73008, Ukraine.

[*] Corresponding Author: Eugene Shkvar. Email: shkvar.eugene@qq.com.

actuators [Corke, Jumper, Post et al. (2002); Corke, Cavalieri and Matlis (2002); Durscher and Roy (2011)].

The plasma actuator consists of two essentially asymmetrically located electrodes, which are separated by a dielectric (Fig. 1). One of the electrodes is open and in contact with air, and the other is completely immersed in the dielectric material. The electrodes are located on the aerodynamic surface along the span of the considered streamlined body and, as a rule, are long and thin.
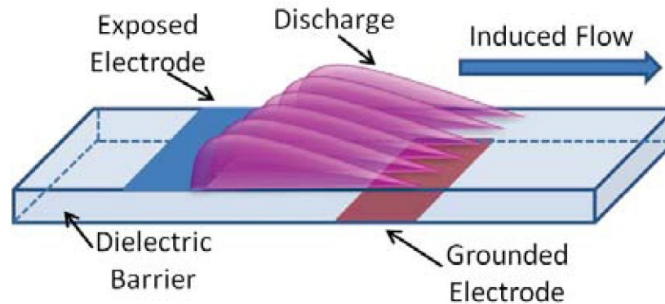

Figure 1: Scheme of a linear plasma actuator [Durscher and Roy (2011)]

Among the methods of plasma control of the air flow structure, the dielectric barrier discharge is considered as one of the most promising for practical application, since it is characterized by stable operation at atmospheric pressure without coagulation of the discharge into a compressed arc. A dielectric barrier discharge is an electrical discharge in a gaseous medium that arises between two electrodes, one or both of which are covered with a dielectric (Fig. 1).

Using a plasma actuator to flow control provides several advantages over mechanical systems. They are entirely electronic, simple in their design, have no moving parts, have low inertia and the ability to integrate into the surface, and can also be located on very thin surfaces.

The plasma actuator has been successfully used in various flow control applications, such as: generation of the boundary layer instability on an sharp cone with Mach 3.5, lift force increase on wing components, flow separation control on low-pressure turbine blades, flow control on a poorly streamlined body, drag reduction, unsteady generation of vortices, flow separation control from the leading edge of the airfoil.

To date, a general understanding of the interaction between the electric field, charged plasma particles and the air has been developed. The electromagnetic field of the plasma actuator is influenced on the charged particles and a mass force (Lorentz force) arises, which leads to the transfer of momentum to the surrounding air.

However, there are significant disagreements about the plasma structure. Plasma structure is extremely important for the description of physics and the operation principle of the dielectric barrier discharge. The complexity of measuring the physical properties of plasma is due to the difference in geometric scales and the significant role of transition processes.

The small size of the plasma region and the transition processes in a dielectric barrier discharge do not allow carry out of direct measurements of the charged particles density.

A large number of experimental [Corke, Jumper, Post et al. (2002); Corke, Cavalieri and Matlis (2002); Durscher and Roy (2011); Massines, Rabehi and Decomps (1998); Thomas, Kozlov and Corke (2006)] and theoretical [Shyy, Jayaraman and Andersson (2002); Hall (2004); Enloe, McLaughlin, VanDyken et al. (2004); Suzen, Huang and Jacob (2005)] works are devoted to the study of a low-temperature nonequilibrium dielectric barrier discharge plasma during operation of a plasma actuator. Researches were conducted in two main directions. The first direction is the study of the physics of a single dielectric barrier discharge. The second direction is the optimization of plasma actuators to increase their efficiency in air flow control. Despite the successful demonstration of the capabilities of a plasma actuator for flow control and the seeming simplicity of the device, a fundamental understanding of the physics of the processes taking place is incomplete.

Theoretical studies of the dielectric barrier discharge are usually based on low-level mathematical models using numerous empirical constants, the values of which depend on the specific type of flow [Shyy, Jayaraman and Andersson (2002); Hall (2004)].

Despite the advantages of a dielectric barrier discharge plasma actuators, their use is still limited to laboratory levels without widespread introduction to modern technology. As a result of the performed experiments, it was established [Corke, Jumper, Post et al. (2002); Corke, Cavalieri and Matlis (2002); Durscher and Roy (2011); Massines, Rabehi and Decomps (1998)] that for effective of flow separation control it is necessary to take into account the geometric and operational characteristics of plasma actuators. These include: actuator location on the streamlined body surface, orientation, geometrical dimensions, relative displacement of the isolated and the open electrodes, applied voltage and its frequency.

The effect of the above parameters on the operation of a plasma actuator makes the optimization of these devices based on experimental studies into a very laborious, complex and expensive task. The use of computational fluid dynamics (CFD) makes it possible to significantly save time and financial costs of optimizing such complex flow control devices.

2 Brief description of chosen object of study and existing experimental data

In this paper we consider a partially ionized quasi-neutral ideal low-temperature nonequilibrium plasma generated by a dielectric barrier discharge in air.

2.1 Equations system of air dynamics

The methodology, developing here, is based on the assumption of low-speed air movement at low Mach numbers ($M < 0.3$), under which the air flow can be considered as an incompressible fluid due to neglecting the of compressibility effects. The dynamics of a viscous incompressible fluid is described by the Reynolds-averaged Navier-Stokes equations with taking into account the additional mass forces, initiated by plasma actuators.

$$\nabla \vec{u} = 0 , \tag{1}$$

$$\frac{\partial \vec{u}}{\partial t} + \left(\vec{u} \cdot \nabla\right)\vec{u} = -\frac{1}{\rho}\nabla p + \nabla\left[\left(\nu + \nu_t\right)\left(\nabla \vec{u}\right)\right] + \frac{1}{\rho}\vec{f}_b,$$ (2)

where ∇ -Hamiltonian operator, t -time, $\vec{u}$ -mean speed vector, p -pressure, ρ -density, ν and ν_t -molecular and turbulent kinematic viscosity coefficients respectively, $\vec{f}_b$ -mass force vector per unit volume.

2.2 Turbulence simulation

To close the system of Reynolds-averaged Navier-Stokes equations, the Spalart-Allmaras differential one-parameter model adapted to the strain rate tensor (Strain-Adaptive Linear Spalart-Allmaras Model-SALSA) [Rung, Bunge, Schatz et al. (2003)] has been applied, which was developed for the problems of external subsonic aerodynamics and is an evolution of the original model Spalart-Allmaras [Spalart and Allmaras (1992)].

2.3 Initial and boundary conditions

For initial conditions determination, the parameters of the undisturbed flow were set in the entire computational domain. Non-reflective boundary conditions were applied on the outer boundary for the calculation of which the method of characteristics was used. A sticking condition was imposed on the surface of a solid body. In the model of turbulence, the value of the working variable on the body was set to zero $\tilde{\nu}_t = 0$, at the inflow boundary condition it was $\tilde{\nu}_t = 0.1$, the Neumann condition was set at the outflow boundary.

2.4 Equations system of plasma electrodynamics

For this class of problems, a plasma can be considered as an ionized quasi-neutral gas [Suzen, Huang and Jacob (2005)]. In general, it can be described by four Maxwell equations:

$$\nabla \cdot \vec{D} = \rho_c,$$ (3)

$$\nabla \cdot \vec{B} = 0,$$ (4)

$$\nabla \times \vec{E} = -\frac{\partial \vec{B}}{\partial t},$$ (5)

$$\nabla \times \vec{H} = j + \frac{\partial \vec{D}}{\partial t},$$ (6)

where $\vec{H}$ -magnetic field strength, $\vec{B}$ -magnetic induction, $\vec{E}$ -electric field strength, $\vec{D}$ -electric induction, j -total electric current density, ρ_c -total electric charge density. Eqs. (3)-(6) are the Gauss's law, the Gauss's law for a magnetic field, the Faraday's law of induction, and Ampère's circuital law with Maxwell's addition, respectively.

It can be assumed [Suzen, Huang and Jacob (2005)] that the charges in the plasma have enough time (as compared to the hydrodynamic time) for redistribution in the region and the system becomes quasistationary. In this case, the electric current j, the magnetic

field strength $\vec{H}$, and the magnetic induction $\vec{B}$ are zero. In addition, the time derivatives of electrical induction $\partial \vec{D} / \partial t$ and magnetic induction $\partial \vec{B} / \partial t$ are zero. Taking into account the information above, from the system of Maxwell's equations there is only one equation $\nabla \cdot \vec{D} = \rho_c$, which is the Gauss's law for electrical induction.

In this case, the Lorentz force, referred to the unit volume, has the form

$$\vec{f}_b = \rho_c \vec{E} \tag{7}$$

and enters the right side of the Navier-Stokes Eq. (2) as a mass force. The vector of electrical induction $\vec{D}$ is related to the vector of electric field strength $\vec{E}$ through the absolute dielectric constant $\varepsilon = \varepsilon_r \varepsilon_o$ and is equal to $\vec{D} = \varepsilon \vec{E}$, where ε_r -relative permittivity; ε_o -vacuum permittivity.

By definition, for the case $\nabla \times \vec{E} = 0$, the electric field strength $\vec{E}$ can be obtained from the gradient of scalar potential Φ. In this case $\vec{E} = -\nabla \Phi$. Then the Gauss's law will take the form

$$\nabla \left(\varepsilon_r \nabla \Phi \right) = -\rho_c / \varepsilon_o . \tag{8}$$

The charge density at any point of the plasma is defined as the difference between the density of the positive and negative charges. Assuming that the plasma is in a quasistationary state, and the time scales are large enough for the redistribution of charges, and applying the Boltzmann relation $n = n_0 \exp\left(e\Phi / kT \right)$, we obtain [Suzen, Huang and Jacob (2005)]

$$\rho_c / \varepsilon_o = -\left(e^2 n_0 / \varepsilon_o \right) \left[\left(1 / kT_i \right) + \left(1 / kT_e \right) \right] \Phi , \tag{9}$$

where T_i и T_e -temperature of ions and electrons in the plasma, respectively.

Using the Debye length λ_D, which characterizes the distance over which the electric field of a separate charge extends in a neutral medium consisting of positively and negatively charged particles

$$\lambda_D = \left[\left(e^2 n_0 / \varepsilon_o \right) \left(1 / kT + 1 / kT_e \right) \right]^{-1/2} , \tag{10}$$

expression (9) takes the form

$$\rho_c / \varepsilon_o = \left(-1 / \lambda_D^2 \right) \Phi . \tag{11}$$

From the moment when gas particles become weakly ionized, it can be assumed that the potential Φ can consist of two parts: the potential from the external electric field ϕ and the potential φ corresponding to the charge density in the plasma [Suzen, Huang and Jacob (2005)]

$$\Phi = \phi + \varphi . \tag{12}$$

If we assume that the Debye length is small and the charge on the wall is small, and the distribution of charged particles in the region is controlled by the potential on the wall

caused by the electric charge on the same wall, then the influence of the very weak plasma electric field on the external electric field can be neglected.

Therefore, we write two separate equations from the point of view of these two potentials, one for the external electric field due to the applied voltage to the electrodes [Suzen, Huang and Jacob (2005)],

$$\nabla\left(\varepsilon_r\nabla\phi\right)=0, \tag{13}$$

and another equation-for the potential acting on the part of charged particles [Suzen, Huang and Jacob (2005)]

$$\nabla\left(\varepsilon_r\nabla\varphi\right)=-\rho_c/\varepsilon_o. \tag{14}$$

Considering expressions (11)-(13), Eq. (14) takes the form

$$\nabla\left(\varepsilon_r\nabla\rho_c\right)=\rho_c/\lambda_D^2. \tag{15}$$

Then, the distribution of potential and charge density is obtaining in the region as a result of solving Eqs. (13) and (15), respectively, the Lorentz force (7) takes the following form

$$\vec{f}_B=\rho_c\vec{E}=\rho_c\left(-\nabla\phi\right). \tag{16}$$

2.5 Initial and boundary conditions for equations system of plasma electrodynamics

As the initial conditions, the zero distribution of the electric potential and the charge density in the region were set.

Eq. (13) is solved for the electric potential using the applied voltage to the electrodes as the boundary condition, as well as the corresponding values of the relative permittivity for air and dielectric. The alternating voltage applied to the open (top) electrode is given as

$$\phi(t)=\phi^{\max}f(t). \tag{17}$$

The waveform function $f(t)$ can be a sine wave

$$f(t)=\sin\left(2\pi\omega t\right) \tag{18}$$

or rectangular

$$\begin{cases} f(t)=1 \quad \textit{для} \quad \sin\left(2\pi\omega t\right)\geq 0, \\ f(t)=-1 \, \textit{для} \quad \sin\left(2\pi\omega t\right)<0, \end{cases} \tag{19}$$

where ω-frequency and $\phi^{\max}$-amplitude of oscillations. A zero potential is applied to the insulated electrode. At the outer boundaries, the Neumann condition is set $\partial\phi/\partial n=0$ [Suzen, Huang and Jacob (2005)].

Eq. (15) is solving for the charge density only in the air domain. The normal gradient for the charge density on the surface of a solid body was assumed to be zero, except for the region above the insulated electrode. At the outer boundary, the charge density was zero. In the area above the insulated electrode, the charge density is described in such a way as to synchronize with the change in time the voltage $\phi(t)$ applied to the open electrode

$$\rho_{c,w}\left(x,t\right)=\rho_c^{\max}G\left(x\right)f\left(t\right), \tag{20}$$

where $\rho_c^{\max}$ -maximum value of the charge density in the region. The change in the charge density $\rho_{c,w}$ on the wall in the insulated electrode direction is described by the function $G(x)$. Experimental studies [Durscher and Roy (2011)] indicate that the distribution of charge density obeys half of the Gaussian distribution

$$G(x) = \exp\left[-(x-\mu)^2 / \left(2\sigma^2\right)\right], \quad for\ x \geq 0, \tag{21}$$

where μ -local parameter indicating the position of the maximum, σ -scale factor determining the decay rate. In the calculations, the local parameter μ is chosen in such a way that the peak of the function $G(x)$ corresponds to the left side of the isolated electrode. The value of the scale factor $\sigma = 0.3$ provides a gradual decrease in the distribution of the charge density from the left side of the electrode to the right. The values of frequency and amplitude applied to the voltage electrodes are taken from experiments. It has been established [Corke, Jumper, Post et al. (2002)], that the Debye length λ_D is equal to 0.0075 m, and the maximum charge density $\rho_c^{\max}$ in the region is assumed to be 0.0075 C/m³.

3 Numerical method

A specialized computational fluid dynamics (CFD) package, based on the Navier-Stokes equations for calculating steady and unsteady laminar and turbulent flows, has been developed by Redchyts [Redchyts (2009)]. For numerical simulation of the dielectric barrier discharge, two equations have been additionally solved. They described the distributions of the applied voltage and density of charged particles. These equations were integrated into the developed CFD package. The impact of the plasma actuator on air was carried out through the Lorentz force (16), which is included as a source term in the Navier-Stokes Eqs. (1), (2).

The system of governing equations of hydrodynamics (1), (2) and electrodynamics (13), (15) was written in an arbitrary curvilinear coordinate system in a dimensionless form. The integration of the system of governing equations was carried out numerically using the finite volume method. For convective terms, the upwind Rogers-Kwak [Rogers, Kwak (1991)] approximation was used on the basis of the third-order Roe scheme. In turbulence models, the TVD scheme with a third-order ISNAS flow limiter was used to approximate convective terms. The derivatives in Eqs. (13), (15) and in viscous terms of Eq. (2) were approximated by a second-order central difference scheme. For equations solving the algorithm, based on a three-layer implicit scheme with subiterations in pseudo-time of the second order of accuracy in physical time, was used. The obtained block-matrix system of linear algebraic equations was solved by the generalized minimal residual (GMRES) method with ILU(k) preconditioning.

4 Results and discussion

4.1 Plasma actuators on the cylinder

Plasma actuators were applied to air flow control on the cylinder. All the initial data for this work are taken from Massines et al. [Massines, Rabehi and Decomps (1998)]. The model is a cylinder made of quartz (D=100 mm), with four plasma actuators arranged as shown in Fig. 2. An alternating voltage of $\phi = 11.5$ kV with a frequency of 10 kHz is applied to the plasma actuators. The walls of the cylinder were 2.5 mm thick. The open electrode is made of copper foil 5.6 mm wide and 0.04 mm thick. The width of the insulated electrode is 25.4 mm, and the thickness is 0.04 mm. The internal dielectric is 5 layers of Kapton 0.125 mm thick. In the present work, numerical simulation of the dielectric barrier discharge during the plasma actuator operation was carried out in a dimensionless form. As characteristic values, $L = 0.1$ m, $U = 1$ m/s, $\rho_\infty = 1.225$ kg/m^3, $\rho_{c\,max} = 0.0075$ C/m^3, $\varphi_{max} = 11500$ V, $\nu_\infty = 1.47 \cdot 10^{-5}$ m^2/s were used.

As a result of the carried out numerical experiment, the distribution of the electric potential and the density of charged particles near the electrodes and in the region was obtained (Fig. 3). The maximum of the charge density is observed in areas with a maximum electric field strength.
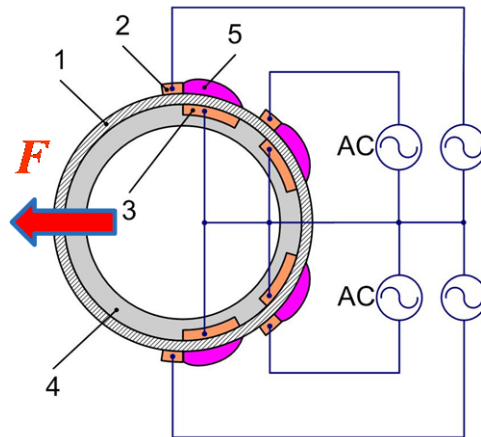

Figure 2: Cylinder model with four plasma actuators [Massines, Rabehi and Decomps (1998)] (1-cylinder, 2-exposed electrode, 3-insulated (grounded) electrode, 4-internal dielectric, 5-plasma areas)

A jet is formed on the back side of the cylinder as a result of the action of four plasma actuators on the quiescent air (Fig. 4). The movement of air leads to a drop in pressure in this area, and the jet is pressed against the surface of the cylinder. The movement of air leads to a pressure decrease in this area, and the jet is pressed to the cylinder surface. Something similar to the Coanda effect arises. In the wake, a jet stream is formed, which leads to the emergence of a propulsion force. The change in the time of propulsion force coefficient of the cylinder is obtained (Fig. 5). The time-averaged propulsion force coefficient is -0.04.
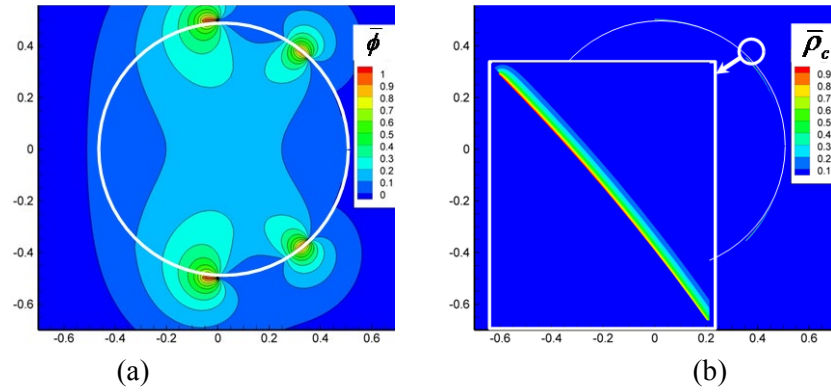
(a)   (b)

Figure 3: The distribution of the electric potential (a) and the charged particles density (b)

(a)   (b)

(c)   (d)
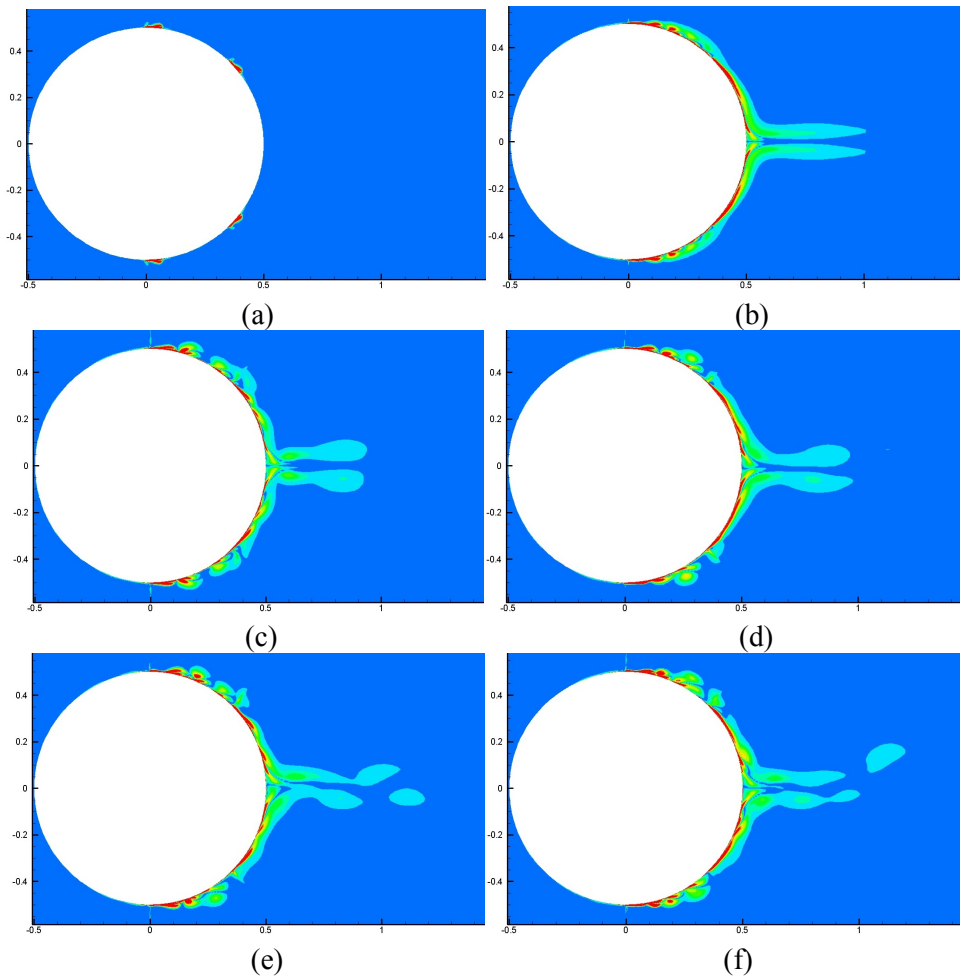
(e)   (f)

Figure 4: Induced by a plasma actuator air flow on the cylinder a) $t=0$; b) $t=5$; c) $t=10$; d) $t=15$; e) $t=20$; f) $t=25$
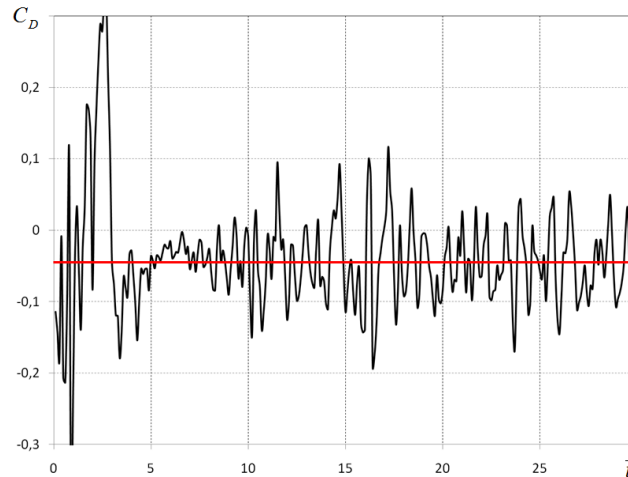
Figure 5: The change in time of the propulsion force coefficient of the cylinder

4.2 Flow separation control on the cylinder using four plasma actuators

In this paper, numerical simulation of effects of four plasma actuators on the air flow around cylinder for the Reynolds number $\mathrm{Re} = 30000$ performed. In order to visualize the flow structure, smoke flow visualization was used in the experiment, and the vorticity module isolines were used in this work.

Turbulent flow around a cylinder is characterized by the presence of a Karman vortex street in the wake (Figs. 6-9). Due to the action of viscous forces near the cylinder surface, the fluid particles lose some of the kinetic energy, which is no longer enough to overcome the pressure increase in the bottom part of the cylinder. A reverse flow is formed near the separation point from which a large vortex develops. After some time, this vortex separates from the cylinder and demolished downstream. In the swirling zone behind the bottom part of the cylinder, the pressure is greatly reduced compared to the pressure in the undisturbed flow. At some distance behind the cylinder, a sequence of vortices rotating alternately in different directions is formed.

The turn-on of four plasma actuators ($\phi = 11.5$ kV), located on the surface of the cylinder, leads to the suppression of the Karman vortex street and the flow around the cylinder is attached (Fig. 10).

The pressure coefficient for various flow regimes around a circular cylinder shows in Fig. 11. The solid line corresponds to a potential non-circulatory flow $C_P = 1 - 4\sin^2 \varphi$. Here, complete restoration of the bottom pressure take place, which, in the absence of friction forces, leads to the d'Alembert paradox (zero drag force). In viscous flows, friction makes a relatively small contribution to to drag force. However, the presence of friction leads to flow separation and a significant redistribution of pressure on the surface of the cylinder. For a developed Karman vortex street, the pressure coefficient values are in the zone indicated by dashed lines in Fig. 11. The suppression of the Karman vortex street with the help of plasma actuators leads to the restoration of bottom pressure and reduction of drag (●●● line in Fig. 11).
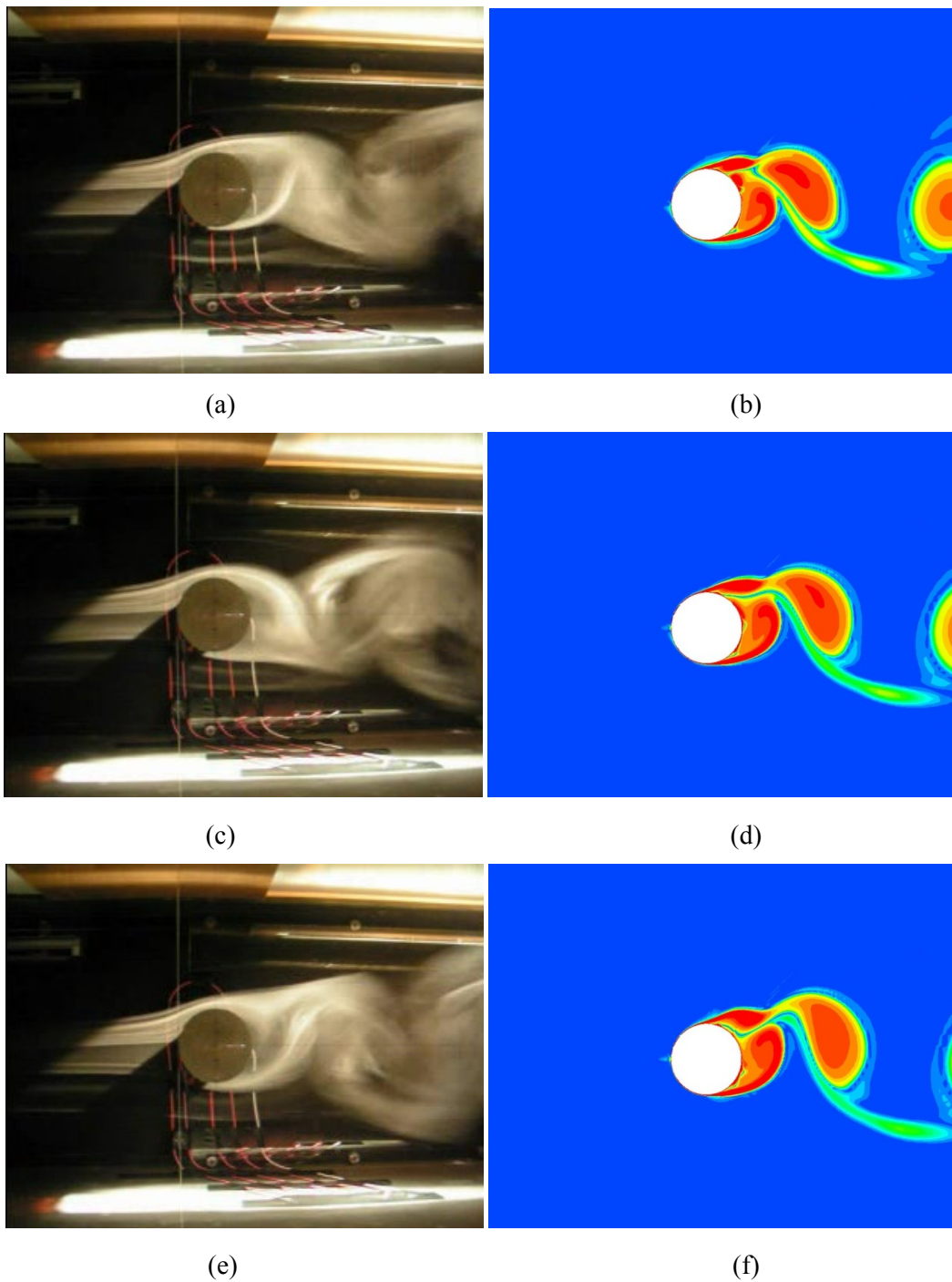
(a)

(b)

(c)

(d)

(e)

(f)

Figure 6: Turbulent flow around cylinder with turned off plasma actuators for dimensionless time moments t=39.5 (a, b), t=39.6 (c, d), t=39.7 (e, f), (a, c, e-experiment [Massines, Rabehi and Decomps (1998)], b, d, f-present work)
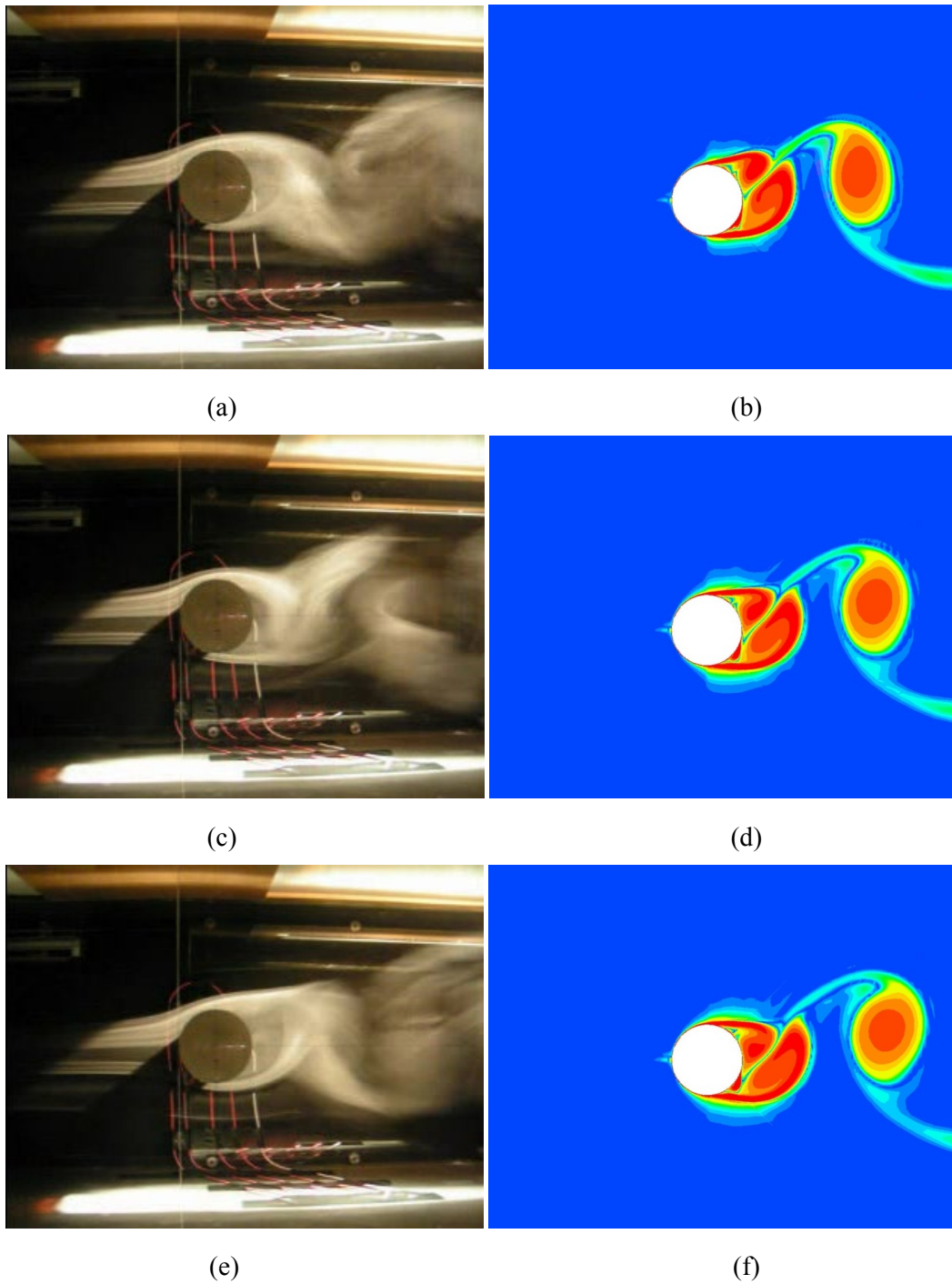
(a)

(b)

(c)

(d)

(e)

(f)

Figure 7: Turbulent flow around cylinder with turned off plasma actuators for dimensionless time moments t=39.8 (a, b), t=39.9 (c, d), t=40.0 (e, f), (a, c, e-experiment [Massines, Rabehi and Decomps (1998)], b, d, f-present work)
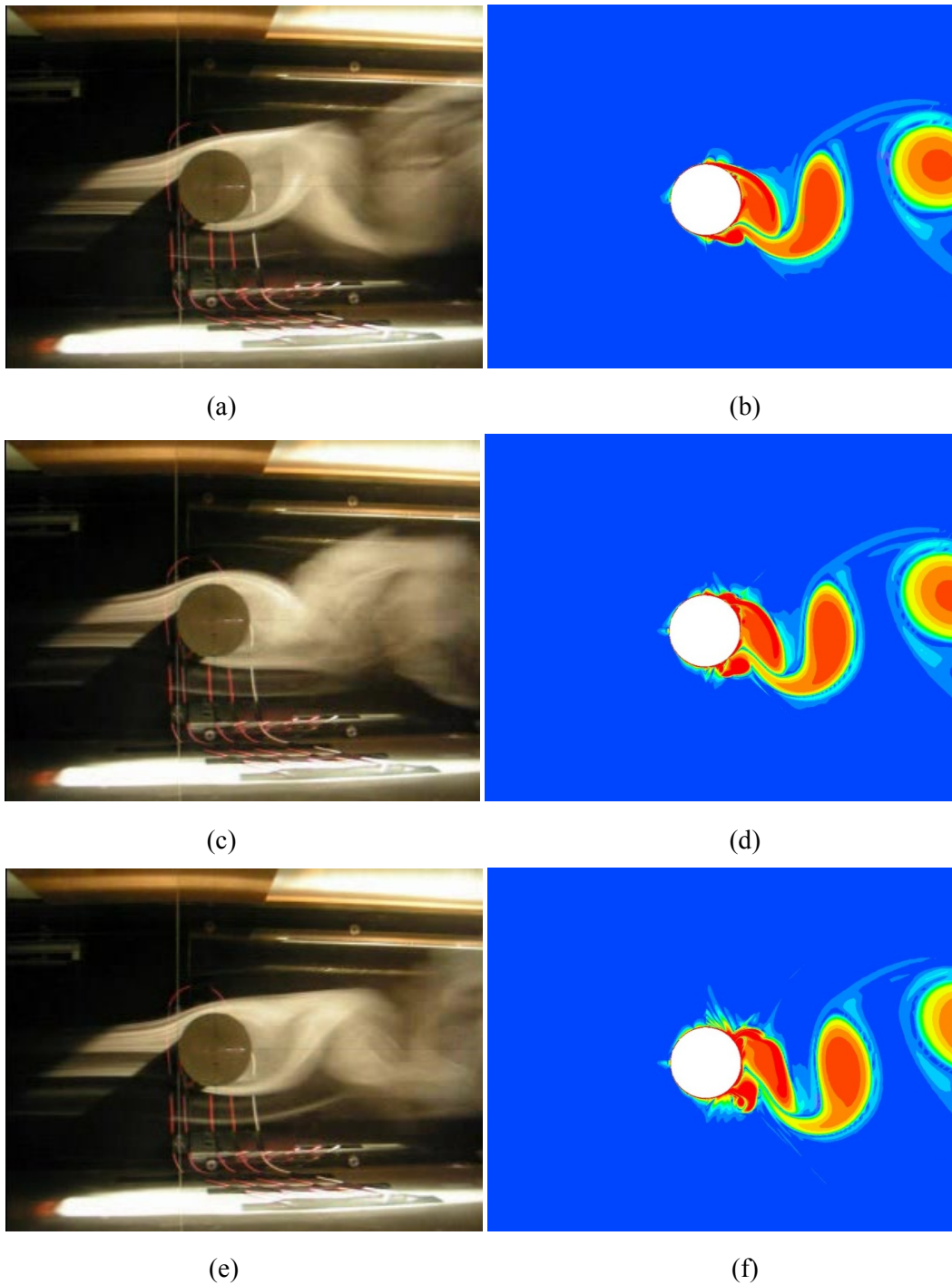
(a)

(b)

(c)

(d)

(e)

(f)

Figure 8: Turbulent flow around cylinder with turned on plasma actuators for dimensionless time moments t=40.1 (a, b), t=40.2 (c, d), t=40.3 (e, f), (a, c, e-experiment [Massines, Rabehi and Decomps (1998)], b, d, f-present work)
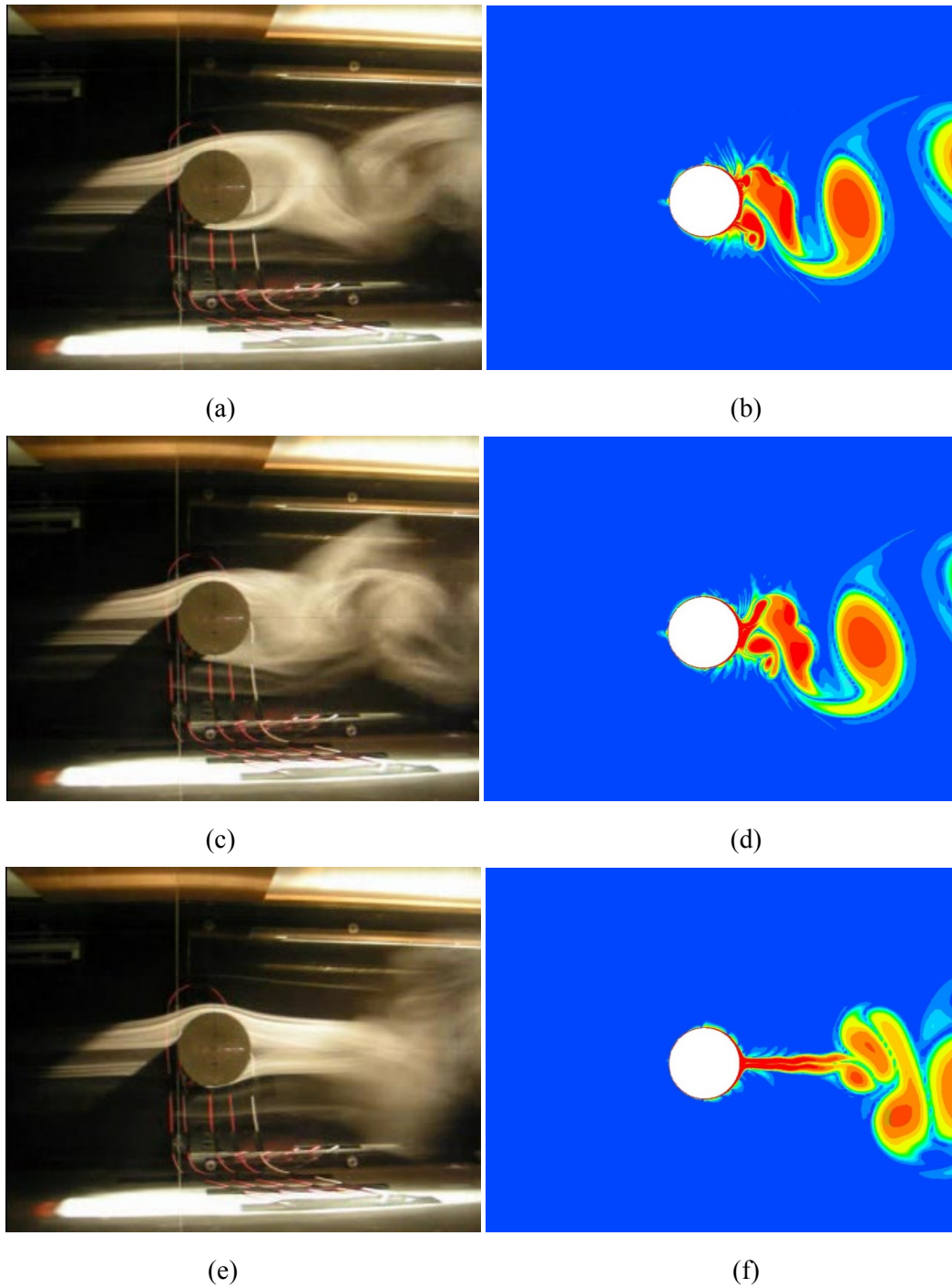
(a)   (b)

(c)   (d)

(e)   (f)

Figure 9: Turbulent flow around cylinder with turned on plasma actuators for dimensionless time moments t=40.4 (a, b), t=40.5 (c, d), t=41.0 (e, f), (a, c, e-experiment [Massines, Rabehi and Decomps (1998)], b, d, f-present work)
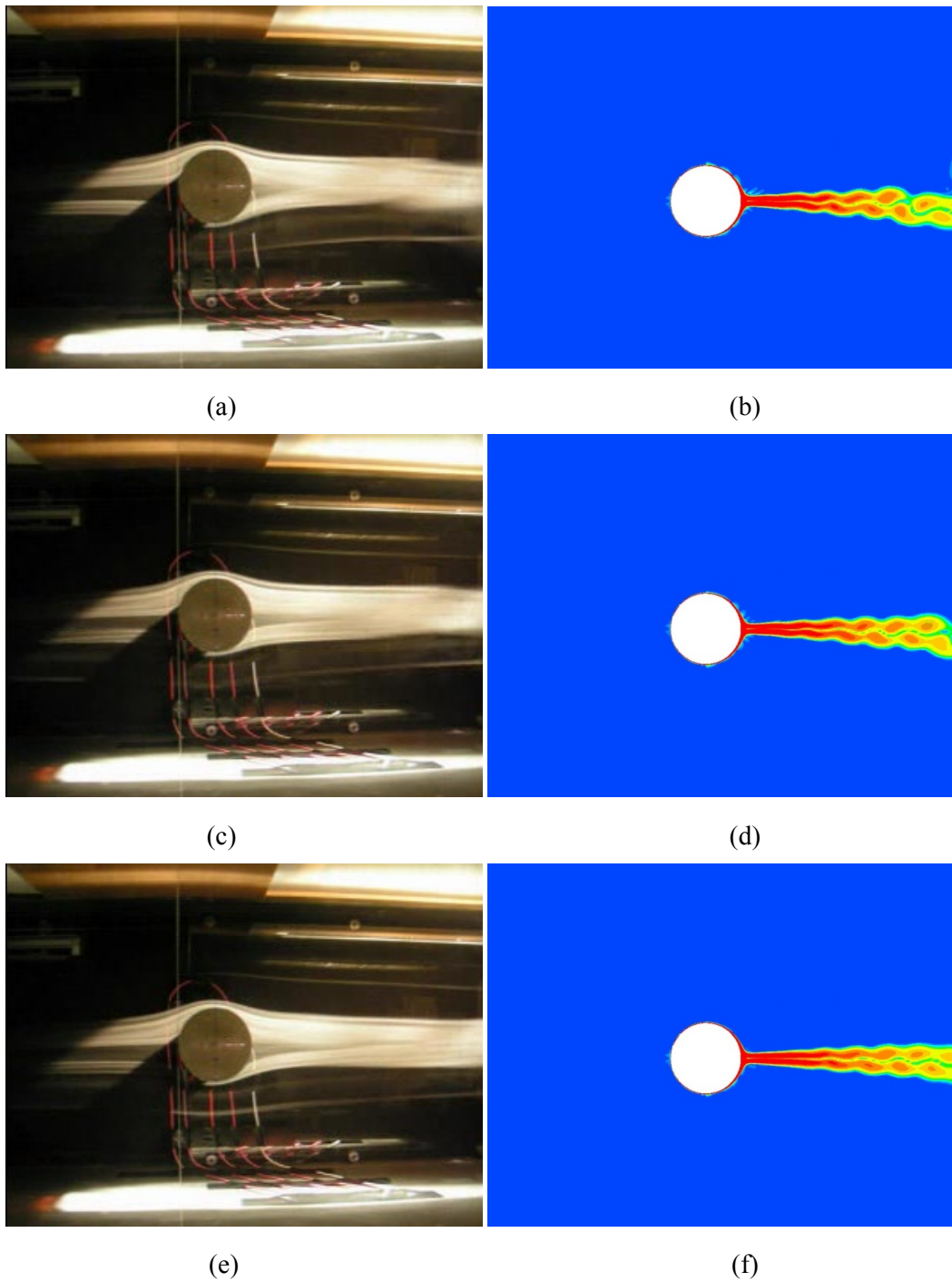
(a)

(b)

(c)

(d)

(e)

(f)

Figure 10: Turbulent flow around cylinder with turned on plasma actuators for dimensionless time moments t=42.0 (a, b), t=43.0 (c, d), t=44.0 (e, f), (a, c, e-experiment [Massines, Rabehi and Decomps (1998)], b, d, f-present work)
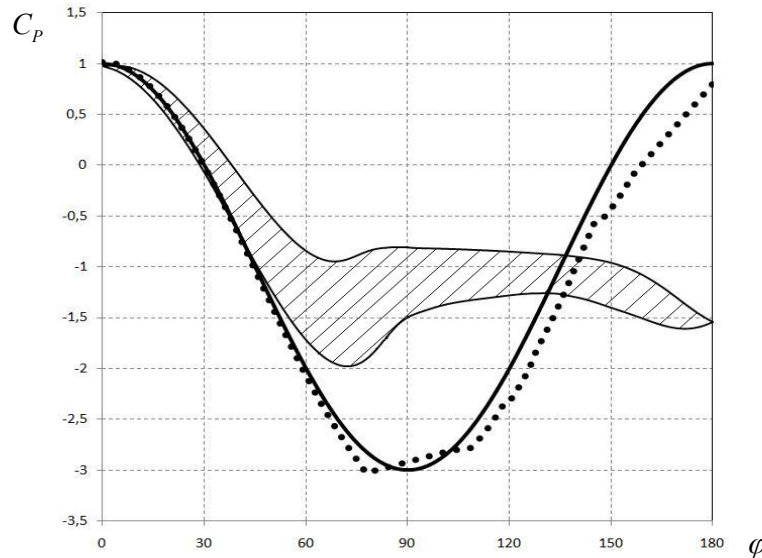
Figure 11: The distribution of the pressure coefficient for different flow regimes of a circular cylinder

Depending on the Reynolds number, the flow regime of the cylinder (laminar, transient, turbulent), the intensity of the plasma actuators, the value of the drag coefficient can decrease from 2 to 10 times. The results obtained for the flow around a cylinder for a case with plasma actuators turned off and turned on satisfactorily coincide with experimental data [Massines, Rabehi and Decomps (1998)] (Figs. 6-10).

5 Conclusion

On the basis of the physical model of the dielectric barrier discharge, the mathematical model describing unsteady electro- and aerodynamic processes during the plasma actuator operation was constructed. The numerical algorithm was developed for solving plasma electrodynamics equations with the equations of viscous incompressible fluid dynamics including turbulence in a curvilinear coordinate system on moving grids to simulate a dielectric barrier discharge. On the basis of the developed approach, the numerical simulation of the occurrence of a propulsion force as a result of the action of plasma actuators on a cylinder in the quiescent air was performed. The possibility of reducing the cylinder drag coefficient with the help of the plasma actuators due to the suppression of the Karman vortex street is shown. The proposed method takes into account the physical features of the considered class of problems and has a high computational efficiency. This approach is applicable to numerical simulation the dynamics of liquid and gas flows in the presence of an electrostatic field.

References

Corke, T.; Cavalieri, D.; Matlis, E. (2002): Boundary layer instability on a sharp cone at Mach 3.5 with controlled input. *AIAA Journal*, vol. 40, no. 5, pp. 1015-1018.

Corke, T.; Jumper, E.; Post, M.; Orlov, D. (2002): Application of weakly ionized plasmas as wing flow control devices. *AIAA Paper*, no. 350, pp. 15.

Durscher, R.; Roy, S. (2011): Induced flow from serpentine plasma actuators acting in quiescent air. *AIAA Paper*, no. 957, pp. 12.

Enloe, C.; McLaughlin, T.; VanDyken, R.; Fuscher, J. (2004): Plasma structure in the aerodynamic plasma actuator. *AIAA Paper*, no. 844, pp. 9.

Gad-El-Hak, M. (2007): *Flow Control: Passive, Active, and Reactive Flow Management.* Cambridge University Press.

Hall, K. (2004): *Potential Flow Model for Plasma Actuation as a Lift Enhancement Device (Ph.D. Thesis)*, pp. 158. University of Notre Dame.

Massines, F.; Rabehi, A.; Decomps, P. (1998): Experimental and theoretical study of a glow discharge at atmospheric pressure controlled by dielectric barrier. *Journal of Applied Physics*, vol. 83, no. 6, pp. 2950-2957.

Redchyts, D. (2009): Numerical simulation of separated flows on the based on unsteady Navier-Stokes equations. *Scientific Statements of Belgorod State University. Series Mathematics Physics*, vol. 17, no. 13, pp. 118-146.

Rogers, S. E.; Kwak, D. (1991): An upwind differencing scheme for the incompressible Navier-Stokes equations. *Journal Numerical Mathematics*, vol. 8, pp. 43-64.

Rung, T.; Bunge, U.; Schatz, M.; Thiele F. (2003): Restatement of the Spalart-Allmaras eddy-viscosity model in strain-adaptive formulation. *AIAA Journal*, vol. 4, no. 7, pp. 1396-1399.

Shkvar, Y. O.; E, S. J.; Kryzhanovskyi, A. S.; Cai, J. (2018): Mathematical modeling of turbulent boundary layers, modified by wall-localized drag reduction techniques. *The Book of Abstracts of the 8th International Conference on Vortex Flows Mechanics*, pp. 29.

Shyy, W.; Jayaraman, B.; Andersson, A. (2002): Modeling of glow discharge-induced fluid dynamics. *Journal of Applied Physics*, vol. 92, no. 3, pp. 6434-6443.

Spalart, P. R.; Allmaras, P. R. (1992): A one-equation turbulence model for aerodynamic flow. *AIAA Paper*, vol. 12, pp. 439-478.

Suzen, Y.; Huang, P.; Jacob, J. (2005): Numerical simulations of plasma based flow control applications. *AIAA Paper*, no. 4633, pp. 14.

Thomas, F.; Kozlov, A.; Corke, T. (2006): Plasma actuators for bluff body flow control. *AIAA Paper*, no. 2845, pp. 16.